nature medicine

PPAR-δ is repressed in Huntington's disease, is required for normal neuronal function and can be targeted therapeutically

Audrey S Dickey[1], Victor V Pineda[2], Taiji Tsunemi[1], Patrick P Liu[3–5], Helen C Miranda[1], Stephen K Gilmore-Hall[1], Nicole Lomas[1], Kunal R Sampat[1], Anne Buttgereit[1], Mark-Joseph Manalang Torres[2], April L Flores[1], Martin Arreola[1], Nicolas Arbez[6], Sergey S Akimov[6], Terry Gaasterland[5,7], Eduardo R Lazarowski[8], Christopher A Ross[6,9–11], Gene W Yeo[3–5], Bryce L Sopher[2], Gavin K Magnuson[12], Anthony B Pinkerton[12], Eliezer Masliah[13,14] & Albert R La Spada[1,3–5,14–16]

Huntington's disease (HD) is a progressive neurodegenerative disorder caused by a CAG trinucleotide repeat expansion in the huntingtin (*HTT*) gene, which encodes a polyglutamine tract in the HTT protein. We found that peroxisome proliferator-activated receptor delta (PPAR-δ) interacts with HTT and that mutant HTT represses PPAR-δ–mediated transactivation. Increased PPAR-δ transactivation ameliorated mitochondrial dysfunction and improved cell survival of neurons from mouse models of HD. Expression of dominant-negative PPAR-δ in the central nervous system of mice was sufficient to induce motor dysfunction, neurodegeneration, mitochondrial abnormalities and transcriptional alterations that recapitulated HD-like phenotypes. Expression of dominant-negative PPAR-δ specifically in the striatum of medium spiny neurons in mice yielded HD-like motor phenotypes, accompanied by striatal neuron loss. In mouse models of HD, pharmacologic activation of PPAR-δ using the agonist KD3010 improved motor function, reduced neurodegeneration and increased survival. PPAR-δ activation also reduced HTT-induced neurotoxicity *in vitro* and in medium spiny-like neurons generated from stem cells derived from individuals with HD, indicating that PPAR-δ activation may be beneficial in HD and related disorders.

The PPARs are ligand-activated transcription factors that belong to the nuclear hormone receptor superfamily. The three subtypes—termed PPAR-α, PPAR-δ and PPAR-γ—serve as lipid sensors in response to increased energy requirements[1]. PPARs are activated by lipids and fatty acid derivatives, and they perform essential functions in lipid homeostasis, glucose metabolism, energy production and cellular differentiation.

The least-studied member of the PPAR nuclear receptor family is PPAR-δ, which shows a fairly ubiquitous expression pattern but is highly abundant in skeletal muscle and brain[2,3]. The function of PPAR-δ has been studied in skeletal muscle, in which PPAR-δ regulates skeletal muscle energy metabolism and mitochondrial biogenesis[4,5]. Indeed, PPAR-δ promotes mitochondrial biogenesis and regulates fiber-type switching in muscle[6,7]. PPAR-δ is at least twofold more highly expressed in brain than in muscle[8], making it the most abundant PPAR subtype in the central nervous system (CNS), but its functional relevance there remains unknown.

HD is a progressive autosomal-dominant neurodegenerative disorder in which individuals develop motor and cognitive impairments[9]. Although the mutant HTT protein is widely expressed, neurodegeneration and atrophy occur principally in the medium-sized spiny neurons (MSNs) of the striatum and in the cerebral cortex pyramidal neurons that project to the striatum[10]. In 1993, a CAG trinucleotide-repeat-expansion mutation in the coding region of the *HTT* gene was identified as the cause of HD[11]. Glutamine tracts (polyQ) in HTT that exceed a certain length threshold (approximately 37 repeats in individuals with HD) adopt a pathogenic conformation, yielding HTT conformers that are resistant to the normal processes of protein turnover, resulting in the accumulation of pathogenic mutant HTT, cellular toxicity and neurodegeneration[12].

Neurons in the brain have high energy demands and require mitochondrial production of ATP. Chronic administration of a mitochondrial toxin, 3-nitropropionic acid, results in selective loss of MSNs in the striatum[13]. This finding has been corroborated in HD cell-culture models, mice and samples from individuals with HD (reviewed in ref. 14), and it has been suggested that mitochondrial dysfunction may underlie HD pathogenesis and may account for the cell-type specificity.

[1]Department of Pediatrics, University of California San Diego, La Jolla, California, USA. [2]Department of Laboratory Medicine, University of Washington, Seattle, Washington, USA. [3]Department of Cellular and Molecular Medicine, University of California San Diego, La Jolla, California, USA. [4]Institute for Genomic Medicine, University of California San Diego, La Jolla, California, USA. [5]Sanford Consortium for Regenerative Medicine, University of California San Diego, La Jolla, California, USA. [6]Division of Neurobiology, Department of Psychiatry, Johns Hopkins University School of Medicine, Baltimore, Maryland, USA. [7]Scripps Institute for Oceanography, University of California San Diego, La Jolla, California, USA. [8]Department of Medicine, University of North Carolina, Chapel Hill, North Carolina, USA. [9]Department of Neurology, Johns Hopkins University School of Medicine, Baltimore, Maryland, USA. [10]Department of Pharmacology, Johns Hopkins University School of Medicine, Baltimore, Maryland, USA. [11]Department of Neuroscience, Johns Hopkins University School of Medicine, Baltimore, Maryland, USA. [12]Sanford-Burnham-Prebys Medical Discovery Institute, La Jolla, California, USA. [13]Department of Pathology, University of California San Diego, La Jolla, California, USA. [14]Department of Neurosciences, University of California San Diego, La Jolla, California, USA. [15]Division of Biological Sciences, University of California San Diego, La Jolla, California, USA. [16]Rady Children's Hospital, San Diego, California, USA. Correspondence should be addressed to A.R.L.S. (alaspada@ucsd.edu).

Received 30 June; accepted 4 November; published online 7 December 2015; doi:10.1038/nm.4003

At the same time, the observation that HTT needs to be localized to the nucleus for HD pathogenesis to occur highlighted nuclear pathology as a potential early step in the neurotoxicity cascade[15]. N-terminal fragments of mutant HTT protein interfere with gene transcription in the early stages of the disease process (reviewed in ref. 16). We and others linked the mitochondrial dysfunction and metabolic defects in HD to the transcriptional dysregulation of PPAR-γ coactivator–1α (PGC-1α), a co-activator that controls a network of transcriptional programs that culminate in mitochondrial biogenesis and enhanced energy production[17–19]. The importance of PGC-1α for HD pathogenesis is underscored by the observation that PGC-1α overexpression in mouse models of HD (hereafter referred to as HD mice) is sufficient to rescue motor phenotypes, reduce accumulation of misfolded HTT protein in the CNS and ameliorate neurodegeneration[20].

In an unbiased screen for HTT-interacting proteins, we found PPARs to be candidate interactors. We then evaluated the different PPARs and documented an interaction between PPAR-δ and HTT. We investigated the role of PPAR-δ repression in HD and determined that transcriptional dysregulation as a consequence of altered PPAR-δ function underlies mitochondrial dysfunction and neurodegeneration in HD. By directing expression of dominant-negative PPAR-δ to the CNS or specifically to MSNs in the striatum of HD mice, we demonstrated that expression of dominant-negative PPAR-δ is sufficient to produce motor phenotypes, neurodegeneration, mitochondrial defects and transcriptional abnormalities that parallel disease phenotypes in HD. In light of these results, we evaluated the PPAR-δ agonist KD3010 as a therapy for HD and found that KD3010 treatment could ameliorate HD phenotypes in transgenic mice and in striatal medium spiny-like neurons derived from induced pluripotent stem cells (iPSCs) from individuals with HD. Our findings offer novel insights into the pathogenesis of HD, provide evidence for an unexpectedly crucial role for PPAR-δ in maintaining neural health and highlight a promising therapeutic strategy for HD and related neurodegenerative disorders.

RESULTS

Huntingtin and PPAR-δ physically interact

To identify transcription factors that interact with HTT, we transfected HEK293 cells with a construct that encodes a GFP-tagged N-terminal human HTT protein containing 25 glutamines (GFP–HTT^{25Q}), immunoprecipitated GFP–HTT^{25Q} and applied the immunoprecipitated material to a transcription factor binding-site array. This unbiased screen yielded PPAR-response element (PPRE)-binding proteins as candidate HTT-interacting proteins (**Supplementary Fig. 1a**) and led us to examine whether HTT interacts with one of the PPARs. To test this hypothesis, we transiently cotransfected HEK293 cells with constructs encoding GFP–HTT^{25Q}, GFP–HTT^{104Q} or GFP alone and those encoding FLAG-tagged PPAR-α, PPAR-δ or PPAR-γ. After immunoprecipitating HTT using GFP-specific antibodies, we performed immunoblot analyses with a FLAG-specific antibody and detected PPAR-δ in immunoprecipitates from cells expressing GFP–HTT^{25Q} or GFP–HTT^{104Q}; however, we found no evidence for an interaction between HTT and PPAR-α or between HTT and PPAR-γ (**Fig. 1a**). Quantification of the intensity of the PPAR-δ–specific band after GFP–HTT immunoprecipitation and immunoblot analysis indicated that the polyglutamine (polyQ)-tract expansion promotes greater interaction between PPAR-δ and HTT (**Supplementary Fig. 1b**). PPAR-δ is the most abundantly expressed PPAR subtype in the CNS[8]; however, its functional relevance in the CNS is not well defined.

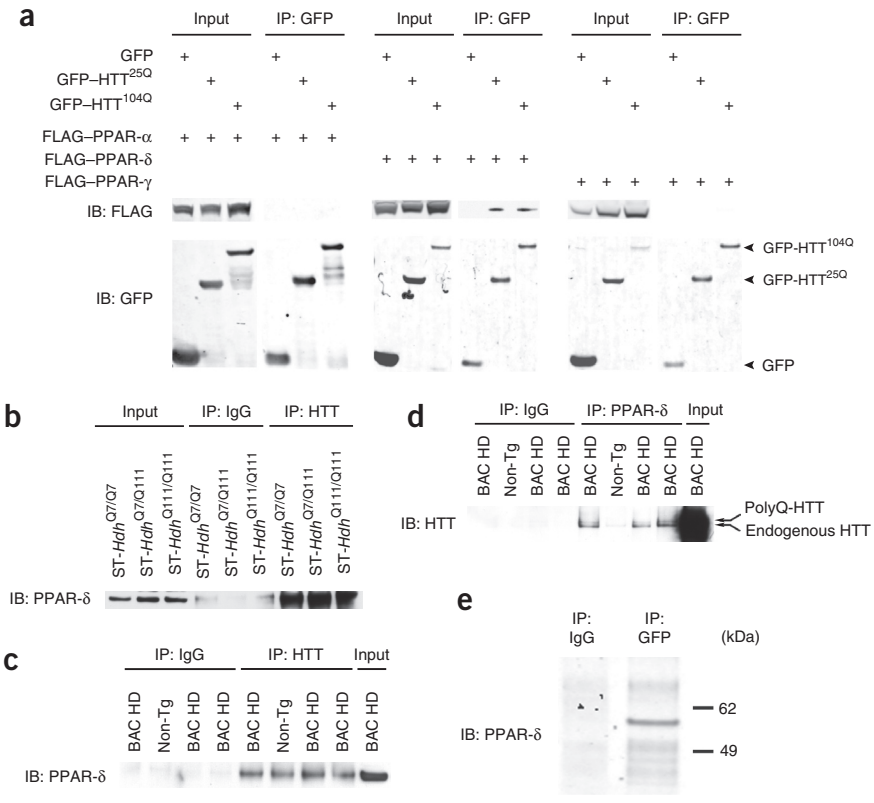

Figure 1 Huntingtin and PPAR-δ physically interact. (**a**) Representative immunoblot analysis ($n = 4$ biological replicates) for FLAG-tagged PPAR-α, PPAR-δ or PPAR-γ after immunoprecipitation of GFP–HTT^{25Q} or GFP–HTT^{104Q} from HEK293 cells expressing constructs encoding the indicated proteins. GFP-only empty vector control–transfected HEK293 cells served as a negative control. (**b**) Representative immunoblot analysis ($n = 4$ biological replicates) for PPAR-δ after immunoprecipitation of HTT from ST-*Hdh* striatal-like neurons of the indicated genotypes. (**c**) Representative immunoblot analysis ($n = 3$ biological replicates) of PPAR-δ after immunoprecipitation from protein lysates of the cortices of 8-month-old BAC-HD97 (BAC HD) mice and nontransgenic (Non-Tg) controls using an HTT-specific antibody. (**d**) Representative immunoblot analysis ($n = 3$ biological replicates) of HTT after immunoprecipitation from protein lysates of the cortices of 8-month-old BAC-HD97 mice or nontransgenic (Non-Tg) controls using an antibody to PPAR-δ. Note the detection of both transgenic polyQ-HTT protein and endogenous mouse HTT protein in BAC-HD97 samples and of endogenous mouse HTT protein in the Non-Tg control. (**e**) Representative immunoblot analysis ($n = 4$ biological replicates) of PPAR-δ after immunoprecipitation using a GFP-specific antibody of *in vitro* transcription-coupled translation of GFP-tagged HTT^{Q25} and PPAR-δ. For **b**–**e**, immunoprecipitation using IgG served as a negative control.

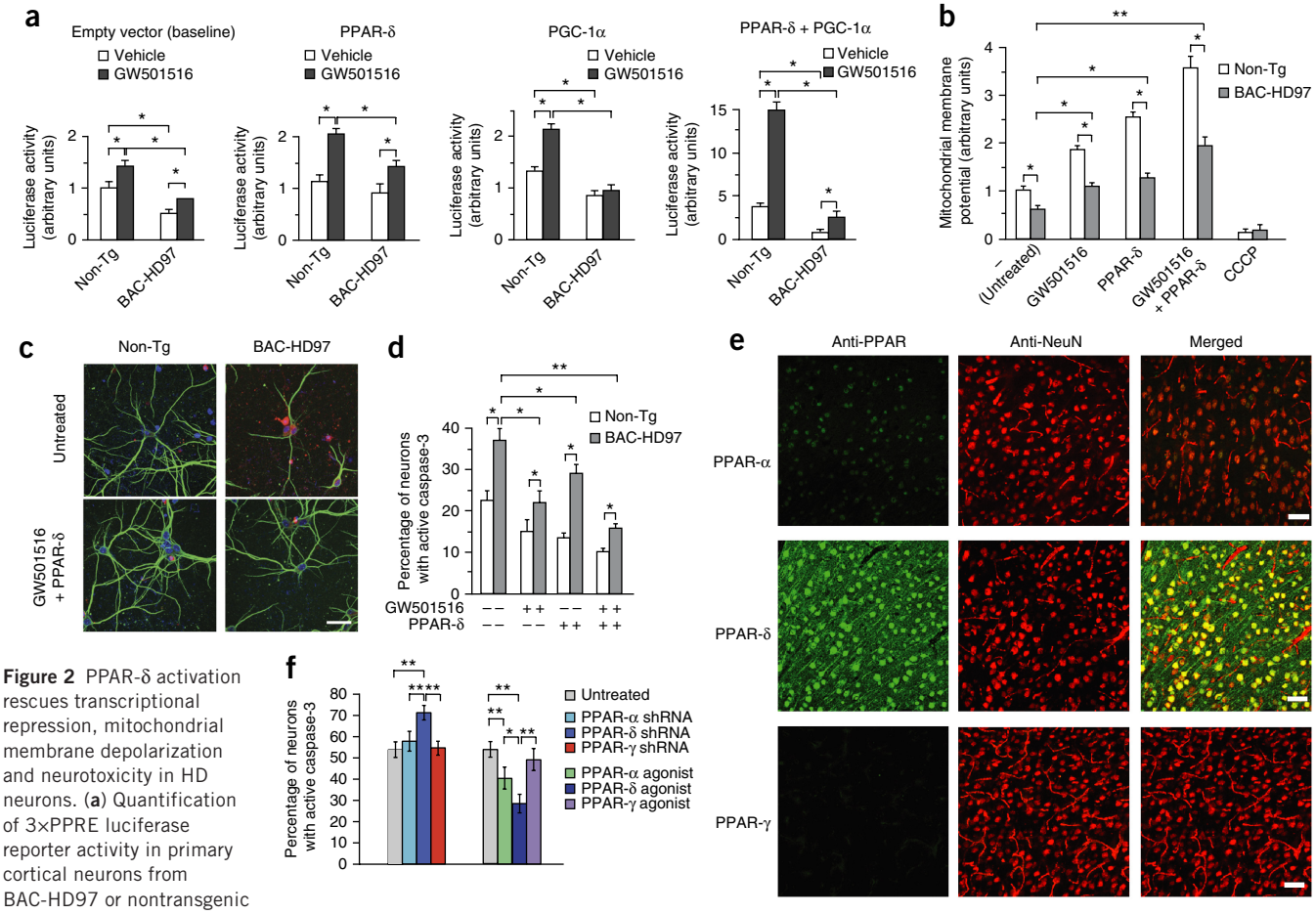

Figure 2 PPAR-δ activation rescues transcriptional repression, mitochondrial membrane depolarization and neurotoxicity in HD neurons. (**a**) Quantification of 3×PPRE luciferase reporter activity in primary cortical neurons from BAC-HD97 or nontransgenic (non-Tg) control mice, cotransfected with a vector expressing *Renilla* luciferase and constructs expressing PPAR-δ and/or PGC-1α, as indicated, and treated with GW501516 (100 nM) or vehicle. Results were normalized to 3×PPRE luciferase reporter activity in non-Tg neurons. $^{*}P < 0.05$; Student's *t*-test. (**b**) Quantification of mitochondrial membrane potential in primary cortical neurons from BAC-HD97 and non-Tg mice, treated as indicated, was determined from the ratio of mitochondrial to cytosolic fluorescence of the potential-sensitive dye, JC-1. Results were normalized to non-Tg neurons at baseline (untreated); carbonyl cyanide *m*-chlorophenyl hydrazone (CCCP) treatment served as a positive control for depolarization. $^{*}P < 0.05$, $^{**}P < 0.01$; Student's *t*-test. (**c**) Representative immunofluorescence images showing active caspase-3 (red) and MAP2 (green) in primary cortical neurons from non-Tg (left) and BAC-HD97 (right) mice that were (bottom) or not (top) transduced with a lentivirus expressing PPAR-δ, and either left untreated (top) or treated with GW501516 (bottom). Scale bar, 20 μm. (**d**) Quantification of neurons displaying active caspase-3 staining from **c**, given as a percentage of the total number of neurons. $^{*}P < 0.05$, $^{**}P < 0.01$; Student's *t*-test. (**e**) Representative images of cortices from non-Tg mice (three sections from each of three mice) immunostained with the indicated PPAR-specific antibody (green; left) and with a NeuN-specific antibody (red; middle). Merged images (right) reveal expression of the indicated PPAR. Scale bars, 50 μm. (**f**) Quantification of the immunofluorescence of active caspase-3 in primary cortical neurons from BAC-HD97 mice that were untreated, transfected with the indicated shRNA construct for 3 d, or treated with 100 nM fenofibrate (PPAR-α agonist), 100 nM GW501516 (PPAR-δ agonist) or 20 nM pioglitazone (PPAR-γ agonist) for 24 h before exposure to 25 μM H_2O_2. $^{*}P < 0.05$, $^{**}P < 0.01$; analysis of variance (ANOVA) with *post hoc* Tukey's test. Throughout, error bars represent mean ± s.e.m. All experiments were performed with three biological replicates and nine technical replicates per condition.

To determine whether endogenous PPAR-δ and HTT interact, we performed coimmunoprecipitations from striatal-like cell lines derived from huntingtin knock-in mice (ST-*Hdh*), which feature equivalent expression of full-length mouse HTT protein with different polyQ tract lengths. After immunoprecipitating HTT with an antibody directed against its C terminus (**Supplementary Fig. 1c**) and immunoblotting with a PPAR-δ–specific antibody, we found that PPAR-δ interacts with full-length HTT in ST-$Hdh^{Q7/Q7}$ (in which both alleles of the knocked-in *Htt* gene at the *Hdh* locus have a polyQ tract of seven glutamines; considered to be wild type (not polyQ expanded)), polyQ-expanded heterozygous ST-$Hdh^{Q7/Q111}$ and polyQ-expanded homozygous ST-$Hdh^{Q111/Q111}$ cells (**Fig. 1b**). To establish whether this interaction occurs in the CNS under physiological conditions, we performed coimmunoprecipitation analyses on protein lysates made from the cortices of BAC-HD97 mice, a highly representative HD mouse model that features proper expression of full-length HTT protein[21]. We immunoprecipitated HTT, performed immunoblot analysis with a PPAR-δ–specific antibody and detected the PPAR-δ protein in the lysates from BAC-HD97 and nontransgenic mice (**Fig. 1c**). We then immunoprecipitated PPAR-δ and performed immunoblot analysis with an HTT-specific antibody; we observed both polyQ-expanded HTT (polyQ-HTT) and endogenous HTT protein in PPAR-δ immunoprecipitates from the cortices of BAC-HD97 mice and detected endogenous HTT in PPAR-δ immunoprecipitates from cortices of nontransgenic mice (**Fig. 1d**). Finally, to determine the nature of the interaction, we performed *in vitro* transcription and translation of PPAR-δ and GFP–HTT^{Q25} (residues 1–171) and then did a pulldown with a GFP-specific antibody or an IgG-isotype control antibody.

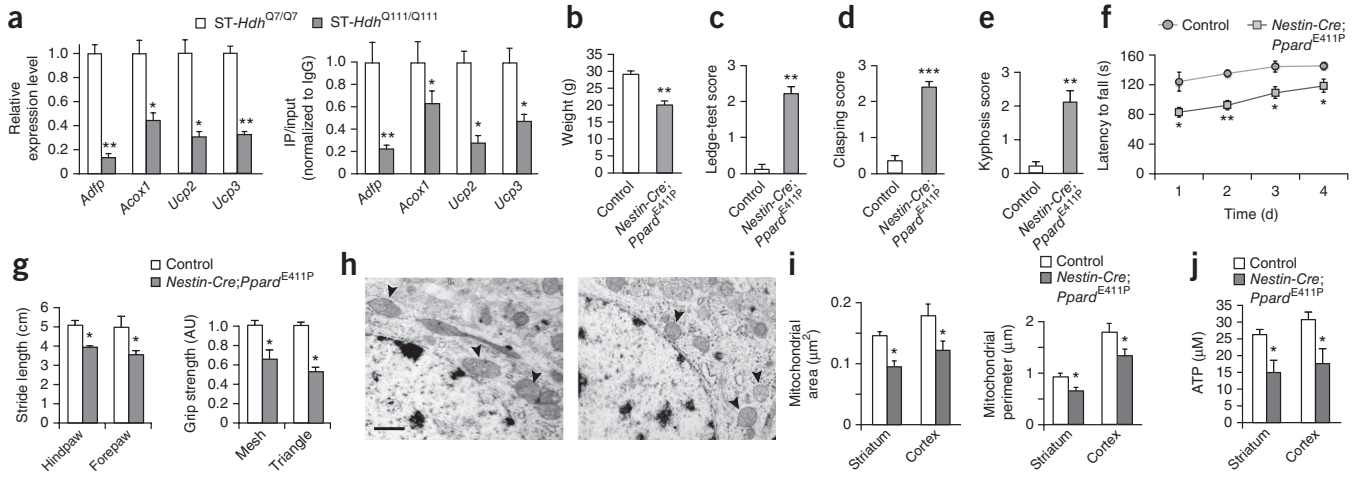

Figure 3 Interference with the transcriptional function of PPAR-δ yields neuron dysfunction and induces neurological phenotypes and mitochondrial abnormalities in transgenic mice. (**a**) Analysis of PPAR-δ target gene expression by RT-PCR (left) and of ChIP for PPAR-δ occupancy at the promoters of PPAR-δ target genes (right) in wild-type ST-*Hdh* (ST-*Hdh*$^{Q7/Q7}$) and homozygous HTT-mutant (ST-*Hdh*$^{Q111/Q111}$) striatal-like cells ($n = 3$ per genotype; 6–9 technical replicates). $^{**}P < 0.01$, $^{*}P < 0.05$; Student's *t*-test. (**b**) Quantification of body weights of *Nestin-Cre*;*Ppard*^{E411P} and littermate control mice. $^{**}P < 0.01$; Student's *t*-test. (**c**) Quantification of cage-ledge tests for *Nestin-Cre*;*Ppard*^{E411P} and littermate control mice showing that *Nestin-Cre*;*Ppard*^{E411P} mice could not easily dismount from the cage ledge. $^{**}P < 0.01$; Student's *t*-test. (**d**) Quantification of clasping tests for *Nestin-Cre*;*Ppard*^{E411P} and littermate control mice showing that *Nestin-Cre*;*Ppard*^{E411P} mice exhibited a prominent clasping phenotype. $^{***}P < 0.001$; Student's *t*-test. (**e**) Quantification of kyphosis for *Nestin-Cre*;*Ppard*^{E411P} and littermate control mice showing that *Nestin-Cre*;*Ppard*^{E411P} mice displayed kyphosis. $^{**}P < 0.01$; Student's *t*-test. (**f**) Quantification of rotarod tests for *Nestin-Cre*;*Ppard*^{E411P} and littermate control mice showing that *Nestin-Cre*;*Ppard*^{E411P} mice attained significantly worse 'latency-to-fall' times on the accelerating rotarod. $^{*}P < 0.05$, $^{**}P < 0.01$; ANOVA with *post hoc* Tukey's test. (**g**) Quantification of stride-length (left) and grip-strength (right) tests for *Nestin-Cre*;*Ppard*^{E411P} and littermate control mice showing decreased mean stride length and reduced combined mesh and triangle grip strength in *Nestin-Cre*;*Ppard*^{E411P} mice. Grip strength is given in arbitrary units with littermate control performance set to 1. $^{*}P < 0.05$; Student's *t*-test. For **b**–**g**, cohort age was 8 months, and group sizes were 8 control mice and 9 *Nestin-Cre*;*Ppard*^{E411P} mice. (**h**) Representative (of 60) electron micrographs of mitochondria in striatum neurons of 8-month-old control (left) and *Nestin-Cre*;*Ppard*^{E411P} (right) mice ($n = 4$ mice per group; 15 micrographs per mouse). Each arrowhead indicates a single mitochondrion. Scale bar, 1 μm. (**i**) Quantification of neuron mitochondrial size in the striatum and cortex, as assessed by measurements of mitochondrial area (left) and perimeter (right) ($n = 4$ mice per group). $^{*}P < 0.05$; Student's *t*-test. (**j**) Quantification of ATP concentrations in the striatum and cortex of 8-month-old mice of the indicated genotypes ($n = 3$ mice per group). $^{*}P < 0.05$; Student's *t*-test. For all experiments, error bars represent mean ± s.e.m.

Immunoblot analysis of the pulled down material showed that PPAR-δ protein was specifically present in the immunoprecipitates obtained by using the GFP-specific antibody (**Fig. 1e**). These findings indicate that PPAR-δ and HTT physically interact in the CNS.

Altered PPAR-δ transactivation contributes to mitochondrial dysfunction and neurotoxicity in HD

We evaluated the effect of polyQ-HTT on PPAR-δ transactivation by cotransfecting constructs expressing an N-terminal fragment of HTT (exons 1 and 2) and a 3×PPRE-luciferase reporter into HEK293 cells and noted a polyQ length–dependent inhibition of PPAR-δ transactivation after treatment with the PPAR-δ–selective agonist GW501516 (**Supplementary Fig. 2a**). We then measured PPAR-δ transactivation in ST-*Hdh* striatal-like cells; we found that PPAR-δ transactivation was significantly repressed ($P < 0.05$) in a polyQ length–dependent manner, that this repression could be partially rescued by expression of either PPAR-δ or PGC-1α and that repression could be fully rescued by expression of both PPAR-δ and PGC-1α (**Supplementary Fig. 2b**). To examine the role of PPAR-δ–dependent transcriptional repression in neurons from HD mice, we repeated the transactivation assays in primary cortical neurons from BAC-HD97 mice (hereafter referred to as BAC-HD97 neurons) and observed significantly impaired PPAR-δ transactivation at baseline, after cotransfection with a construct encoding PPAR-δ or PGC-1α, and in response to cotransfection with constructs expressing PPAR-δ and PGC-1α (**Fig. 2a**). We measured mitochondrial membrane potential (MMP) and noted significantly reduced MMP in BAC-HD97 neurons (**Fig. 2b**). Notably, overexpression of PPAR-δ (via infection of cells with a PPAR-δ–encoding lentivirus) or treatment of cells with GW501516 rescued the mitochondrial membrane–polarization alterations in BAC-HD97 neurons, and the combination of PPAR-δ overexpression and GW501516 treatment resulted in the most robust effect (**Fig. 2b**). Activation of caspase-3, an enzymatic mediator of apoptosis, was elevated, and immunoreactivity of microtubule-associated protein (MAP) 2, which reflects neuron health, was reduced in BAC-HD97 neurons, as compared to that in primary cortical neurons from nontransgenic mice, indicating that HD neurons are more susceptible to cell death (**Fig. 2c**). We noted increased MAP2 staining and reduced caspase-3 activation in BAC-HD97 neurons that were transduced with the PPAR-δ–encoding lentivirus, in the presence of GW501516 (**Fig. 2c**). Increased PPAR-δ expression, GW501516 treatment or the combination of PPAR-δ expression and GW501516 treatment rescued cell death in BAC-HD97 neurons (**Fig. 2d**). Analysis of MAP2 immunoreactivity in BAC-HD97 neurons independently corroborated these results (**Supplementary Fig. 2c**).

We have previously shown that altered transcriptional activity of PGC-1α contributes to HD pathogenesis, with significant reductions in the expression of PGC-1α targets in mice or humans with HD[19]. Although the expression of PGC-1α is reduced in HD, the magnitude of the decrease cannot fully account for the transcriptional alterations documented in HD, indicating that a PGC-1α–dependent transcription factor could be responsible for the transcriptional dysregulation. Because PPAR-δ and HTT physically interact in the CNS and because specific PPAR-δ target genes exhibit reduced expression in the striatum

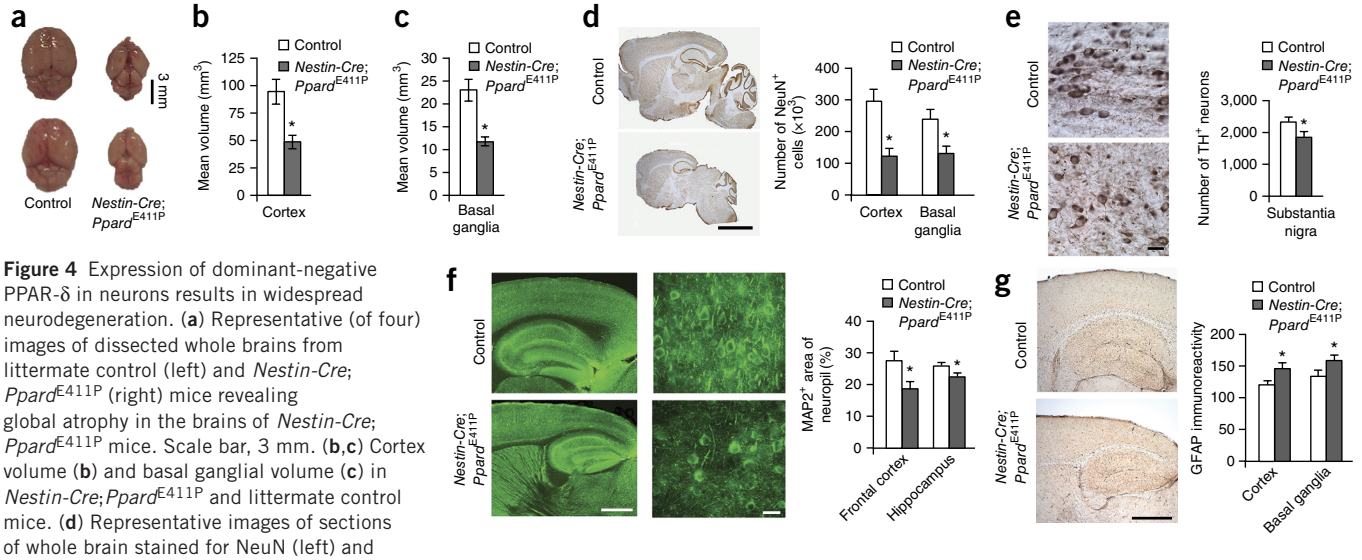

Figure 4 Expression of dominant-negative PPAR-δ in neurons results in widespread neurodegeneration. (**a**) Representative (of four) images of dissected whole brains from littermate control (left) and *Nestin-Cre*; *Pparδ*^{E411P} (right) mice revealing global atrophy in the brains of *Nestin-Cre*; *Pparδ*^{E411P} mice. Scale bar, 3 mm. (**b**,**c**) Cortex volume (**b**) and basal ganglial volume (**c**) in *Nestin-Cre*;*Pparδ*^{E411P} and littermate control mice. (**d**) Representative images of sections of whole brain stained for NeuN (left) and quantification of neuron number (right) for the indicated mice. Scale bar, 250 μm. (**e**) Representative images of TH staining (left) and quantification of TH$^+$ dopaminergic neurons (right) in the substantia nigra of *Nestin-Cre*;*Pparδ*^{E411P} and littermate control mice. Scale bar, 10 μm. (**f**) Left, representative low-magnification (left; scale bar, 100 μm) and high-magnification (right; scale bar, 10 μm) images of the frontal cortex and hippocampus stained for MAP2. Right, quantification of MAP2 immunoreactivity as a percentage of the overall neuropil. (**g**) Representative images (left) and quantification (right) of overall GFAP immunoreactivity in the cortex and basal ganglia. Scale bar, 100 μm. Throughout, cohort age was 10 months; group sizes were 4 control mice and 6 *Nestin-Cre*;*Pparδ*^{E411P} mice; all representative images in **d**–**g** were obtained from sets of three sections per mouse for each group. Error bars represent mean ± s.e.m.; $^*P < 0.05$; Student's *t*-test.

from BAC-HD97 mice, we postulated that impaired PPAR-δ function accounts for altered PGC-1α transcriptional activity in HD. Gene set analysis of Affymetrix U133A/B microarray expression data from the striata of individuals with HD revealed significant alterations in 12 of 16 principal PPAR-δ target genes ($P < 10^{-4}$, chi-squared test; **Supplementary Fig. 3a**), consistent with this hypothesis.

Physical interaction of polyQ-HTT with PPAR-δ promotes HD neurotoxicity

To determine the physiological relevance of the interaction between PPAR-δ and HTT, we examined striatal sections from HD N171^{82Q} transgenic mice (in which the HTT N-terminal fragment has 82 glutamines) and observed colocalization of polyQ-HTT protein with PPAR-δ (**Supplementary Fig. 3b**). To test whether disruption of this interaction could prevent polyQ-HTT–dependent neurotoxicity, we created expression constructs encoding PPAR-δ with deletions of different domains (**Supplementary Fig. 4a**). We cotransfected HEK293 cells with expression constructs encoding GFP-tagged HTT or domain-deleted PPAR-δ, performed co-immunoprecipitation analyses and mapped the HTT interaction site to the D domain (hinge region) of PPAR-δ (**Supplementary Fig. 4b**). To determine whether the physical interaction between polyQ-HTT and PPAR-δ is necessary for neurotoxicity, we co-expressed different PPAR-δ deletion mutants in combination with full-length PPAR-δ in ST-*Hdh*$^{Q111/Q111}$ striatal-like cells. Although co-expression of PPAR-δ lacking either the A–C domains or the E–F domains prevented polyQ-HTT–mediated transcriptional repression, mitochondrial membrane depolarization and cell death, co-expression of PPAR-δ lacking the D–F domains did not rescue any of these neurotoxicity phenotypes (**Supplementary Fig. 5**). These findings indicate that the PPAR-δ deletion constructs that specifically retain the D domain can compete for binding to the mutant HTT and that this binding is sufficient to blunt polyQ-HTT–mediated neurotoxicity, thus underscoring the importance of the PPAR-δ–mutant HTT interaction for HD pathology.

Previous studies have implicated PPAR-γ–mediated transcriptional alterations in HD pathogenesis[22–24]. To examine the potential contribution of PPAR-α or PPAR-γ dysfunction to polyQ-HTT–mediated neurotoxicity, we surveyed PPAR expression in the CNS. Immunohistochemical analysis of sections from the cortices of control mice revealed prominent neuronal expression of PPAR-δ, modest neuronal expression of PPAR-α and barely detectable neuronal expression of PPAR-γ (**Fig. 2e**). In the cortex, striatum and cerebellum of BAC-HD97 mice and nontransgenic littermates, we observed prominent neuronal expression of PPAR-δ and limited expression of PPAR-α or PPAR-γ (**Supplementary Fig. 6**). These findings were corroborated by immunoblot analyses of cortical lysates, cortical neurons, cerebellar lysates and cerebellar granule neurons from BAC-HD97 and nontransgenic mice (**Supplementary Fig. 7a–d**). To directly determine the contributions of the different PPARs to polyQ-HTT–mediated neurotoxicity, we cultured primary cortical neurons from BAC-HD97 mice and monitored cell death after knocking down expression of *Pparδ*, *Pparα* or *Pparγ* (which encode PPAR-δ, PPAR-α and PPAR-γ, respectively) or after agonist-mediated activation of each PPAR. Cell death was increased in BAC-HD97 neurons in which *Pparδ* expression was silenced by using short hairpin RNAs (shRNAs), whereas knockdown of *Pparα* or *Pparγ* did not affect cell death (**Fig. 2f**). Similarly, treatment of cells with a PPAR-δ agonist reduced cell death, as compared to BAC-HD97 neurons treated with an agonist to PPAR-α or to PPAR-γ (**Fig. 2f**).

To evaluate the contribution of PPAR-δ–dependent transcriptional alterations to HD pathogenesis *in vivo*, we measured the expression of 11 PPAR-δ target genes in the striatum of BAC-HD97 transgenic mice and noted reduced expression for all of the tested PPAR-δ target genes (**Supplementary Fig. 7e**). RT-PCR analysis confirmed significant reductions in the expression levels of PPAR-δ targets in ST-*Hdh*$^{Q111/Q111}$ striatal-like cells, as compared to ST-*Hdh*$^{Q7/Q7}$ cells (**Fig. 3a**). We then performed chromatin immunoprecipitation and found that PPAR-δ occupancy is reduced at the promoters of its target

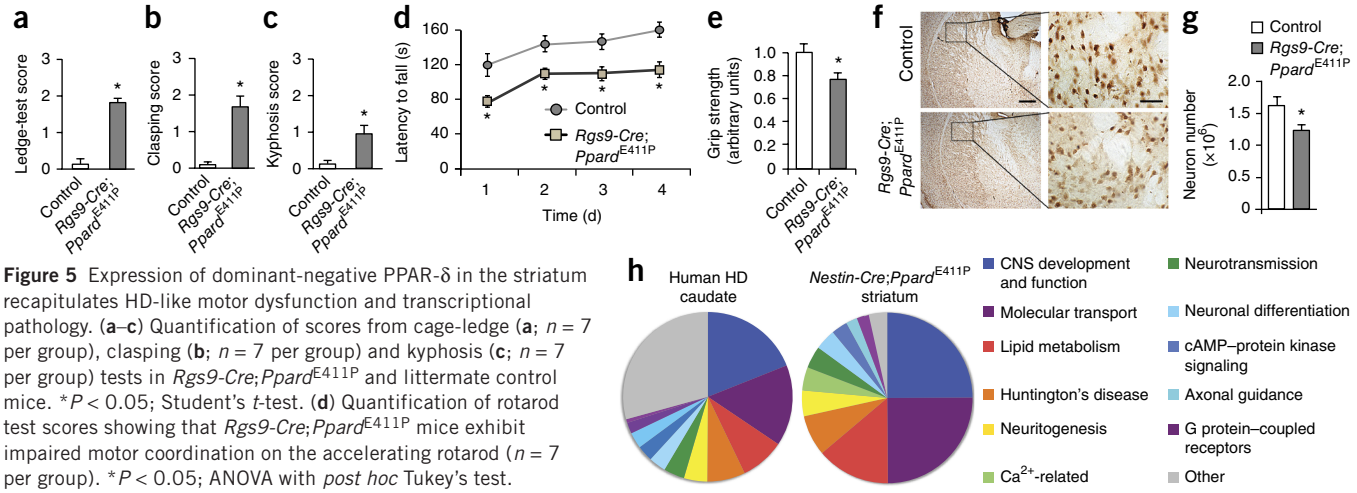

Figure 5 Expression of dominant-negative PPAR-δ in the striatum recapitulates HD-like motor dysfunction and transcriptional pathology. (**a**–**c**) Quantification of scores from cage-ledge (**a**; $n = 7$ per group), clasping (**b**; $n = 7$ per group) and kyphosis (**c**; $n = 7$ per group) tests in *Rgs9-Cre*;*Ppard*^{E411P} and littermate control mice. $^*P < 0.05$; Student's *t*-test. (**d**) Quantification of rotarod test scores showing that *Rgs9-Cre*;*Ppard*^{E411P} mice exhibit impaired motor coordination on the accelerating rotarod ($n = 7$ per group). $^*P < 0.05$; ANOVA with *post hoc* Tukey's test. (**e**) Analysis of mesh grip–strength ($n = 7$ per group). Grip strength is given in arbitrary units with littermate control performance set to 1. $^*P < 0.05$; *t*-test. For **a**–**e**, cohort age was 9 months. (**f**,**g**) Representative images of sections of striatum from 10-month-old *Rgs9-Cre*;*Ppard*^{E411P} mice (bottom) and littermate controls (top) immunostained for NeuN (**f**) and quantification of neuron numbers (**g**) ($n = 4$ mice per group; sets of at least three sections per mouse per group for representative images). Representative insets indicate reduced striatal neuron number in *Rgs9-Cre*;*Ppard*^{E411P} mice. Scale bars, 200 μm and 20 μm (inset). $^*P < 0.05$; Student's *t*-test. (**h**) RNA-seq analysis on striatum from 10-month-old *Nestin-Cre*;*Ppard*^{E411P} mice and littermate control mice ($n = 3$ per group). Pie charts indicate the percentage of genes for the highest ranked altered 'Biofunctions' pathways in microarray expression data from human HD caudate[35] (left) and RNA-seq analysis of *Nestin-Cre*;*Ppard*^{E411P} mouse striatum (right). Throughout, error bars represent mean ± s.e.m.

genes in ST-*Hdh*$^{Q111/Q111}$ striatal-like cells (**Fig. 3a**), suggesting that PPAR-δ binding to target promoters is prevented after its interaction with polyQ-HTT.

Dominant-negative PPAR-δ expression in the CNS induces neurological disease

To determine whether impaired PPAR-δ transactivation function is sufficient to elicit neurodegeneration *in vivo*, we derived a conditional transgenic *Ppard* construct that encodes PPAR-δ with a single amino acid mutation, a substitution of proline for glutamate at residue 411 (*Ppard*^{E411P}) (**Supplementary Fig. 8a**). The *Ppard*^{E411P} mutation results in the inhibition of PPAR-δ transactivation in a dominant-negative manner[25,26]. After generating transgenic mice for *Ppard*^{E411P} such that a combined β-actin promoter–cytomegalovirus (CMV) enhancer and a STOP cassette, flanked by *loxP* sites, is placed 5′ to the *Ppard*^{E411P} cDNA (hereafter referred to as CAGGS-floxed STOP-*Ppard*^{E411P} mice), we evaluated these mice for signs of systemic or neurological phenotypes and did not detect any evidence of abnormality. We then crossed these mice with mice expressing the Cre recombinase under the control of the CMV promoter (*CMV-Cre* driver mice) to permit widespread expression of *Ppard*^{E411P}. Similarly to *Ppard*–knockout mice[27], we found that ubiquitous expression of the PPAR-δ^{E411P} protein causes prenatal lethality. We next crossed the CAGGS-floxed STOP-*Ppard*^{E411P} mice with *Nestin-Cre* mice to obtain double-transgenic *Nestin-Cre*;*Ppard*^{E411P} mice, in which the *Nestin-Cre* driver promotes expression of the Cre recombinase throughout the neural lineage[28]. PPARδ^{E411P} protein was expressed at 1.5- to 2-fold the levels of the endogenous PPAR-δ protein. Characterization of *Nestin-Cre*;*Ppard*^{E411P} mice, in comparison to single-transgenic *Nestin-Cre* or CAGGS-floxed STOP-*Ppard*^{E411P} mice, indicated that *Nestin-Cre*;*Ppard*^{E411P} double-transgenic mice appear smaller by 4–6 months of age, such that by 8 months of age they weigh less than littermate controls (**Fig. 3b**). Phenotype evaluation using a neurological examination screening tool[29] revealed that *Nestin-Cre*;*Ppard*^{E411P} mice suffer prominent motor abnormalities by 8 months of age (**Fig. 3c**–**e**). Testing of the *Nestin-Cre*;*Ppard*^{E411P} mice on an accelerating rotarod confirmed motor impairment (**Fig. 3f**), and stride-length analysis and grip-strength testing provided further evidence for motor abnormalities (**Fig. 3g**). We also evaluated learning and memory in *Nestin-Cre*;*Ppard*^{E411P} mice and documented reduced novel-object recognition and reduced novel-environment exploration (**Supplementary Fig. 8b**–**d**).

Ultrastructural analysis of *Nestin-Cre*;*Ppard*^{E411P} mice revealed that mitochondria in the striatum appear smaller in size (**Fig. 3h**), in agreement with previous studies of HD[30,31], as the mitochondrial area and perimeter in the cortex and striatum were reduced (**Fig. 3i**). To evaluate metabolic function, we measured the activities of mitochondrial complexes. Although the activities of mitochondrial complex I and complex II from *Nestin-Cre*;*Ppard*^{E411P} and control mice were similar, the activities of mitochondrial complex IV and complex V were reduced in the striatum of *Nestin-Cre*;*Ppard*^{E411P} mice (**Supplementary Fig. 9a**–**d**), and the overall ATP concentration was reduced in the striatum and cortex (**Fig. 3j**). Quantitative PCR analysis of mitochondrial and nuclear genomic DNA content corroborated the abnormalities in mitochondrial bioenergetics in the *Nestin-Cre*;*Ppard*^{E411P} mice (**Supplementary Fig. 9e**).

Brain size in adult *Nestin-Cre*;*Ppard*^{E411P} mice was markedly reduced in comparison to that of littermate controls (**Fig. 4a**). Comparable reductions in the volumes of the cortex and the basal ganglia were noted in the *Nestin-Cre*;*Ppard*^{E411P} mice (**Fig. 4b**,**c**). Staining the brain sections of *Nestin-Cre*;*Ppard*^{E411P} mice for the neuronal marker NeuN revealed reduced neuron numbers (**Fig. 4d**). This was paralleled by a reduction in tyrosine hydroxylase (TH)-positive dopaminergic neurons in the substantia nigra (**Fig. 4e**), decreased MAP2 immunostaining in the cortex and hippocampus (**Fig. 4f**), and reactive gliosis, as assessed by glial fibrillary acidic protein (GFAP)-specific immunostaining in the brains of *Nestin-Cre*;*Ppard*^{E411P} mice (**Fig. 4g**). Thus, mice expressing a dominant-negative version of PPAR-δ in the CNS develop striking neurological abnormalities in the context of profound neurodegeneration.

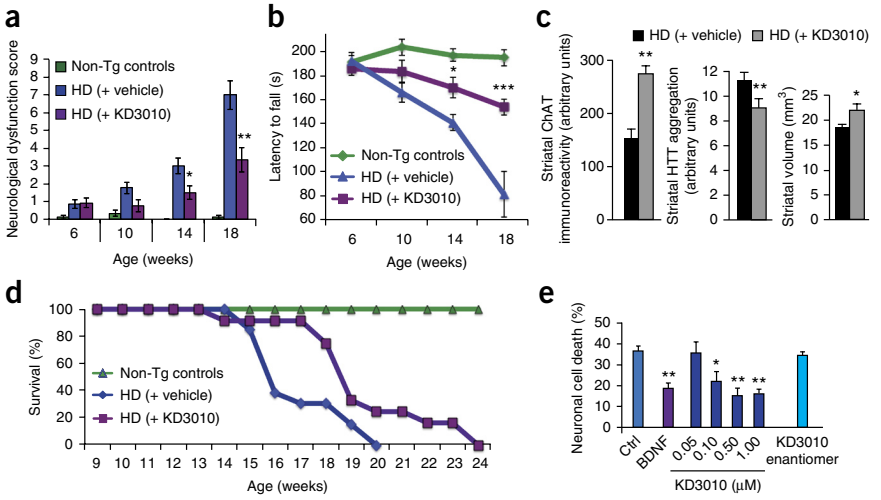

Figure 6 Treatment with the PPAR-δ agonist KD3010 improves motor function, neurodegeneration and survival in HD mice, and KD3010 treatment rescues neurotoxicity in human HD neurons. (**a**,**b**) Composite neurological examination (**a**) and accelerating rotarod analysis (**b**) of HD mice (treated with vehicle (n = 13) or KD3010 (n =12)) and non-Tg littermate controls (n = 9), at the indicated ages. $^{*}P < 0.05$, $^{**}P < 0.01$, $^{***}P < 0.001$; ANOVA with *post hoc* Tukey's test. (**c**) Evaluation of neuropathology in striatum. Quantification of striatal choline acetyltransferase (ChAT) immunoreactivity (n = 4 mice per group) (left), striatal HTT aggregation as assessed by the HTT-specific antibody EM48 (n = 5 mice per group) (middle) and striatal volume by stereology (n = 5 mice per group) (right) for 18-week-old HD mice receiving vehicle or KD3010. $^{*}P < 0.05$, $^{**}P < 0.01$; Student's t-test. (**d**) Kaplan-Meier plot reveals extended lifespan in HD mice receiving KD3010. $^{*}P < 0.05$; log-rank test. (**e**) Quantification of neuronal cell death for medium spiny-like neurons that were differentiated from iPSC lines derived from an individual with HD who has an HTT^{60Q} allele and treated with KD3010 at the indicated concentrations. Neurons treated with 20 ng/ml brain-derived neurotrophic factor (BDNF) were used as a positive control. Untreated neurons, or those treated with the inactive enantiomer of KD3010 at 1 μM, were used as negative controls (Ctrl) (n = 3 per group). $^{*}P < 0.05$, $^{**}P < 0.01$; ANOVA with *post hoc* Bonferroni test. Throughout, error bars represent mean ± s.e.m.

Dominant-negative PPAR-δ expression in the striatum induces HD-like phenotypes

To assess the effect of dominant-negative PPAR-δ–dependent transcriptional interference in the striatum only, we obtained the *Rgs9-Cre* mouse line, which restricts expression of Cre recombinase to striatal MSNs[32], and derived double-transgenic *Rgs9-Cre*;*Ppard*^{E411P} mice. Although the *Rgs9-Cre*;*Ppard*^{E411P} mice are of similar size and weight as gender-matched littermate controls, the *Rgs9-Cre*;*Ppard*^{E411P} mice develop motor abnormalities, as assessed by composite neurological examination[29], rotarod analysis and grip-strength testing (**Fig. 5a**–**e**). Neuropathological examination of *Rgs9-Cre*;*Ppard*^{E411P} mice revealed evidence for decreased numbers of striatal neurons (**Fig. 5f**,**g**), owing to a reduction in parvalbumin-immunoreactive neurons, as acetylcholinesterase-positive neurons were spared (**Supplementary Fig. 10**). This pattern is consistent with striatal neuron loss observed in individuals with HD[33,34]. Because the CAGGS-floxed STOP-*Ppard*^{E411P} transgenic crosses with the *Nestin-Cre* and *Rgs9-Cre* driver lines yielded distinct patterns of neurodegeneration that reflect Cre recombinase expression, the observed phenotypes cannot be attributed to insertional mutagenesis.

Another defining feature of HD pathogenesis is transcriptional abnormalities[16]. We used RNA-seq analysis to assess the striatal transcriptomes of *Nestin-Cre*;*Ppard*^{E411P} mice and found that 583 genes in the striatum from these mice were altered in their expression, as compared to littermate controls. We performed Gene Ontology database analysis on this 583-gene set, identified altered Biofunctions pathways and represented these pathways in proportion to the percentage of the total number of genes whose expression was altered for each significantly perturbed pathway (**Fig. 5h**). To determine whether the transcriptomic changes found in the striatum of *Nestin-Cre*;*Ppard*^{E411P} mice overlap with the changes observed in brains from individuals with HD, we performed Gene Ontology database analysis on the genes whose expression was altered in the caudate of individuals with HD[35], and we represented the detected Biofunctions pathways in proportion to the percentage of the total number of genes whose expression was altered for each pathway (**Fig. 5h**). We ascribed an order to the altered Biofunctions pathways for the human HD caudate transcriptome and the *Nestin-Cre*;*Ppard*^{E411P} striatum transcriptome (**Supplementary Table 1**) and observed nearly identical Biofunctions pathway rankings ($P < 10^{-11}$). To validate gene expression alterations identified by RNA-seq analysis, we performed qRT-PCR analysis on striatal RNAs from *Nestin-Cre*;*Ppard*^{E411P} mice for 11 genes, and documented altered expression for 10 of the 11 tested genes, all in the predicted direction (**Supplementary Fig. 11a**). Finally, to assess the specificity of polyQ-HTT repression of PPAR-δ, we performed assays with the 3×PPRE reporter in HEK293 cells transfected with constructs that encode ataxin-7^{10Q} or ataxin-7^{92Q}—the protein variants associated with a different CAG polyQ-repeat disorder, spinocerebellar ataxia type 7. We found that cells expressing ataxin-7^{92Q} did not repress PPAR-δ transactivation (**Supplementary Fig. 11b**).

The PPAR-δ agonist KD3010 rescues neurological phenotypes and neurodegeneration

PPAR-δ–selective compounds have been identified as potential therapies for type 2 diabetes and metabolic syndrome[36]. KD3010 ((*S*)-4-[*cis*-2,6-dimethyl-4-(4-trifluoromethoxy-phenyl)-piperazine-1-sulfonyl]-indan-2-carboxylic acid tosylate) is a highly selective and potent PPAR-δ agonist[37]. Treatment with KD3010 (in the low-nanomolar range) rescued dominant-negative PPAR-δ–mediated transcriptional repression and mitochondrial dysfunction in BAC-HD97 neurons and could prevent cell death in primary cortical neurons transfected with a 586-residue N-terminal HTT fragment containing 82 glutamines (**Supplementary Fig. 12a**–**c**). Intraperitoneal (i.p.) injection of KD3010 (15 mg per kg of body weight (mg/kg)) into C57BL/6J mice resulted in a ratio of KD3010 in the brain to KD3010 in the plasma of ~10% at 2- to 24-h after injection (**Supplementary Table 2**). To test whether KD3010 treatment could promote PPAR-δ transactivation in the brains of living mice, we injected KD3010 at 50 mg/kg per day (mg/kg/d) and found that this treatment induced the expression of PPAR-δ target genes (**Supplementary Fig. 12d**). KD3010 treatment did not cause weight loss or visible side effects,

and we did not find any evidence of organ toxicity. Hence, KD3010 treatment at 50 mg/kg/d is tolerated in mice and can promote the PPAR-δ transactivation function in the mammalian CNS.

The HD N171^{82Q} mouse model recapitulates HD-like motor phenotypes and neurodegeneration within a time frame of 5–6 months[38]. Beginning at 6 weeks of age, HD mice were injected with either 50 mg/kg/d of KD3010 or vehicle, five times per week. Of note, we adhered to recommended preclinical trial guidelines, which are intended to avoid spurious results[39,40]. We tracked the progression of the disease phenotypes in vehicle-treated and agonist-treated HD mice by performing composite neurological examination[29], rotarod analysis and grip-strength testing at 4-week intervals. KD3010 treatment attenuated neurological dysfunction and improved motor function in HD mice, as compared to vehicle-treated controls (**Fig. 6a**,**b** and **Supplementary Fig. 12e–g**). Striatal choline acetyltransferase (ChAT) levels, which are used as a measure of striatal interneuron dysfunction in HD[33], were increased, aggregated HTT protein was reduced and striatal volume was maintained in KD3010-treated HD mice (**Fig. 6c** and **Supplementary Fig. 13**). In addition to attenuating neurological phenotypes and neurodegeneration, KD3010 treatment yielded a 16% extension in mean lifespan of HD mice (**Fig. 6d**). Finally, we differentiated iPSCs from individuals with HD into striatal medium spiny-like neurons and treated these human HD medium spiny-like neurons with KD3010. Whereas treatment with the inactive enantiomer of KD3010 did not offer any protection from cell death, treatment with KD3010 rescued cell death in neurons derived from individuals with HD (**Fig. 6e**).

DISCUSSION

Here we document PPAR-δ–mediated transcriptional interference as a cause of the bioenergetics defects and mitochondrial abnormalities in HD. In addition to demonstrating that HTT represses PPAR-δ transactivation in an interaction-dependent manner to yield mitochondrial defects and neurotoxicity in a variety of model systems, we generated transgenic mice expressing dominant-negative PPAR-δ to recapitulate HD-like behavioral, metabolic and transcriptional phenotypes. Because interfering with PPAR-δ function in mice can phenocopy HD, our findings implicate PPAR-δ dysregulation as a key node in the HD pathogenic cascade.

Of the three PPARs, the least-studied member of this family is PPAR-δ. We found that treatment with a PPAR-δ–selective agonist evoked a robust response in transactivation assays, and we demonstrated that PPAR-δ could elicit neuroprotection in primary neurons from mouse models of HD. To clarify the role of PPAR-δ with respect to that of PPAR-α and PPAR-γ, we modulated each PPAR individually using shRNA knockdown or agonist treatment and found that only PPAR-δ modulation yielded highly significant effects on HD neurotoxicity. We documented that PPAR-δ is much more highly expressed than PPAR-α or PPAR-γ in neurons of the cortex and striatum, in agreement with previous work[41]. Although studies have shown that treatment with a PPAR-γ agonist can ameliorate disease phenotypes in HD[22,42,43], the beneficial effects of PPAR-γ–agonist therapy probably stem from improved function in peripheral tissues, hypothalamic neurons and non-neural CNS cells[41]. Because our studies suggested an important role for PPAR-δ in neural function, we generated lines of conditional transgenic PPAR-δ mice and directed expression of dominant-negative PPAR-δ to neurons throughout the CNS or just to striatal MSNs. These experiments revealed that PPAR-δ is necessary for normal neural function, as profound neurological and neurodegenerative phenotypes emerged in mice expressing dominant-negative PPAR-δ in neural lineages. Our findings thus identify neurons as a cell type in which PPAR-δ is essential for homeostasis.

We theorized that if impaired PPAR-δ function is contributing to HD pathogenesis, then an attractive treatment option would be to agonize PPAR-δ. Of the various possible PPAR-δ agonists, we opted to use KD3010, as this PPAR-δ agonist is potent and specific, crosses the blood-brain barrier and was approved for use in humans in a Phase 1b metabolic disease safety trial in which no incidences of side effects were reported. We performed a preclinical trial of KD3010 treatment in HD N171^{82Q} transgenic mice and observed compelling evidence for therapeutic efficacy. To further evaluate KD3010 as a treatment for HD, we tested KD3010 in striatal medium spiny-like neurons derived from human iPSCs from individuals with HD and documented robust neuroprotection in the nanomolar range. Our findings strongly suggest that repurposing PPAR-δ agonists that are capable of crossing the blood-brain barrier is a viable treatment strategy for HD and that treatment with KD3010 should be pursued as a lead. Because mitochondrial dysfunction and transcription interference with PGC-1α, the co-activator for PPAR-δ, are recognized features of Parkinson's disease (PD) pathogenesis[44,45] and because we observed marked loss of TH$^+$ dopaminergic neurons in the substantia nigra of dominant-negative PPAR-δ conditional transgenic mice, we note that PPAR-δ–agonist therapy should also be considered as a treatment for PD.

Another facet of PPAR-δ biology with relevance to therapy development for neurodegenerative disease is that PPAR-δ forms a heterodimer with the retinoid X receptor (RXR), and RXR agonists are capable of promoting PPAR-δ transactivation[46]. Bexarotene, a synthetic drug approved for use in humans, is structurally similar to retinoic acid compounds that are known endogenous RXR ligands. One provocative study reported that administration of bexarotene to a mouse model of Alzheimer's disease (AD) yielded dramatic improvements in cognitive, social and olfactory deficits, accompanied by improved neural circuit function and enhanced clearance of soluble Aβ oligomers[47]. Because PPAR-δ is highly expressed in neurons of the CNS[8] and because bexarotene can potently activate PPAR-δ, our results indicate that enhanced PPAR-δ activation could be contributing to bexarotene-mediated neuroprotection in AD[47,48].

Because the PPAR-δ–PGC-1α pathway promotes the expression of genes that drive high-level energy production and insure protein and organelle quality control, the neuroprotective effects of agonizing this pathway probably stem from boosting neuronal bioenergetics and proteostasis. HD, PD and AD are all late-onset disorders, implying that a decline in the function of crucial homeostatic pathways with age is a central factor in the development of clinical disease. In HD, this view is all the more relevant, as affected individuals express the mutant, disease-associated protein from the time of conception, yet they can live for more than five or even six decades without obvious symptoms. It seems reasonable to propose that activation of pathways promoting energy production (which is always under high demand in neurons and CNS cells) and supporting protein and organelle quality control (which constitutes a major challenge for neurons and other CNS cell types) may stave off cellular decompensation in the face of proteotoxic stress during this long prodromal phase. Thus, therapies directed at boosting PPAR-δ function could have broad applicability for a wide range of neurodegenerative diseases.

METHODS

Methods and any associated references are available in the online version of the paper.

Accession codes. Gene Expression Omnibus: *Ppard*^{E411P} striatum transcriptome data are available under accession code GSE74583.

Note: Any Supplementary Information and Source Data files are available in the online version of the paper.

ACKNOWLEDGMENTS

We are grateful to S. Luquet (Université Paris Diderot) for the gift of the CAGGS-floxed-STOP-*Ppard* expression construct. ST-*Hdh* cells were a kind gift from M. MacDonald[20,49] (Massachusetts General Hospital). BAC-HD97 mice[21] were originally obtained from X.W. Yang (David Geffen School of Medicine at UCLA). This work was supported by funding from the Hereditary Disease Foundation, the Cure Huntington's Disease Initiative and grants from the US National Institutes of Health (R01 NS065874 (A.R.L.S.), R01 AG033082 (A.R.L.S.), National Research Service Award F32 NS081964 (A.S.D.) and P01 HL110873 (E.R.L.)).

AUTHOR CONTRIBUTIONS

A.R.L.S. provided the conceptual framework for the study. A.S.D., V.V.P., T.T., B.L.S., E.R.L., G.W.Y., C.A.R., G.K.M., A.B.P., E.M. and A.R.L.S. designed the experiments. A.S.D., V.V.P., P.P.L., H.C.M., S.K.G.-H., N.L., K.R.S., A.B., M.-J.M.T., A.L.F., M.A., N.A., S.S.A., T.G., B.L.S., E.R.L., G.W.Y., E.M., G.K.M., A.B.P. and A.R.L.S. performed the experiments. A.S.D. and A.R.L.S. wrote the manuscript.

COMPETING FINANCIAL INTERESTS

The authors declare no competing financial interests.

1. Berger, J. & Moller, D.E. The mechanisms of action of PPARs. *Annu. Rev. Med.* **53**, 409–435 (2002).
2. Auboeuf, D. *et al.* Tissue distribution and quantification of the expression of mRNAs of peroxisome proliferator-activated receptors and liver X receptor-α in humans: no alteration in adipose tissue of obese and NIDDM patients. *Diabetes* **46**, 1319–1327 (1997).
3. Kliewer, S.A. *et al.* Differential expression and activation of a family of murine peroxisome proliferator-activated receptors. *Proc. Natl. Acad. Sci. USA* **91**, 7355–7359 (1994).
4. Luquet, S. *et al.* Peroxisome proliferator-activated receptor–δ controls muscle development and oxidative capability. *FASEB J.* **17**, 2299–2301 (2003).
5. Schuler, M. *et al.* PGC1-α expression is controlled in skeletal muscles by PPAR-β, whose ablation results in fiber-type switching, obesity and type 2 diabetes. *Cell Metab.* **4**, 407–414 (2006).
6. Wang, Y.X. *et al.* Regulation of muscle fiber type and running endurance by PPAR-δ. *PLoS Biol.* **2**, e294 (2004).
7. Narkar, V.A. *et al.* AMPK and PPAR-δ agonists are exercise mimetics. *Cell* **134**, 405–415 (2008).
8. Girroir, E.E. *et al.* Quantitative expression patterns of peroxisome proliferator-activated receptor-β/δ (PPAR-β/δ) protein in mice. *Biochem. Biophys. Res. Commun.* **371**, 456–461 (2008).
9. Nance, M.A. Genetic testing of children at risk for Huntington's disease. *Neurology* **49**, 1048–1053 (1997).
10. Ross, C.A. *et al.* Huntington's disease and dentatorubral-pallidoluysian atrophy: proteins, pathogenesis and pathology. *Brain Pathol.* **7**, 1003–1016 (1997).
11. The Huntington's Disease Collaborative Research Group. A novel gene containing a trinucleotide repeat that is expanded and unstable on Huntington's disease chromosomes. *Cell* **72**, 971–983 (1993).
12. La Spada, A.R. & Taylor, J.P. Repeat expansion disease: progress and puzzles in disease pathogenesis. *Nat. Rev. Genet.* **11**, 247–258 (2010).
13. Beal, M.F. *et al.* Neurochemical and histologic characterization of striatal excitotoxic lesions produced by the mitochondrial toxin 3-nitropropionic acid. *J. Neurosci.* **13**, 4181–4192 (1993).
14. Lin, M.T. & Beal, M.F. Mitochondrial dysfunction and oxidative stress in neurodegenerative diseases. *Nature* **443**, 787–795 (2006).
15. Saudou, F., Finkbeiner, S., Devys, D. & Greenberg, M.E. Huntingtin acts in the nucleus to induce apoptosis but death does not correlate with the formation of intranuclear inclusions. *Cell* **95**, 55–66 (1998).
16. Riley, B.E. & Orr, H.T. Polyglutamine neurodegenerative diseases and regulation of transcription: assembling the puzzle. *Genes Dev.* **20**, 2183–2192 (2006).
17. Cui, L. *et al.* Transcriptional repression of PGC-1α by mutant huntingtin leads to mitochondrial dysfunction and neurodegeneration. *Cell* **127**, 59–69 (2006).
18. Lin, J. *et al.* Defects in adaptive energy metabolism with CNS-linked hyperactivity in PGC-1α–null mice. *Cell* **119**, 121–135 (2004).
19. Weydt, P. *et al.* Thermoregulatory and metabolic defects in Huntington's disease transgenic mice implicate PGC-1α in Huntington's disease neurodegeneration. *Cell Metab.* **4**, 349–362 (2006).
20. Tsunemi, T. *et al.* PGC-1α rescues Huntington's disease proteotoxicity by preventing oxidative stress and promoting TFEB function. *Sci. Transl. Med.* **4**, 142ra97 (2012).
21. Gray, M. *et al.* Full-length human mutant huntingtin with a stable polyglutamine repeat can elicit progressive and selective neuropathogenesis in BACHD mice. *J. Neurosci.* **28**, 6182–6195 (2008).
22. Chiang, M.C. *et al.* Modulation of energy deficiency in Huntington's disease via activation of the peroxisome proliferator-activated receptor–γ. *Hum. Mol. Genet.* **19**, 4043–4058 (2010).
23. Jin, Y.N., Hwang, W.Y., Jo, C. & Johnson, G.V. Metabolic state determines sensitivity to cellular stress in Huntington disease: normalization by activation of PPAR-γ. *PLoS One* **7**, e30406 (2012).
24. Quintanilla, R.A., Jin, Y.N., Fuenzalida, K., Bronfman, M. & Johnson, G.V. Rosiglitazone treatment prevents mitochondrial dysfunction in mutant huntingtin–expressing cells: possible role of peroxisome proliferator-activated receptor–γ (PPAR-γ) in the pathogenesis of Huntington disease. *J. Biol. Chem.* **283**, 25628–25637 (2008).
25. Bastie, C., Luquet, S., Holst, D., Jehl-Pietri, C. & Grimaldi, P.A. Alterations of peroxisome proliferator-activated receptor–δ activity affect fatty acid–controlled adipose differentiation. *J. Biol. Chem.* **275**, 38768–38773 (2000).
26. Holst, D., Luquet, S., Kristiansen, K. & Grimaldi, P.A. Roles of peroxisome proliferator-activated receptors–δ and –γ in myoblast transdifferentiation. *Exp. Cell Res.* **288**, 168–176 (2003).
27. Peters, J.M. *et al.* Growth, adipose, brain and skin alterations resulting from targeted disruption of the mouse peroxisome proliferator-activated receptor–β(δ). *Mol. Cell. Biol.* **20**, 5119–5128 (2000).
28. Tronche, F. *et al.* Disruption of the glucocorticoid receptor gene in the nervous system results in reduced anxiety. *Nat. Genet.* **23**, 99–103 (1999).
29. Guyenet, S.J. *et al.* A simple composite phenotype scoring system for evaluating mouse models of cerebellar ataxia. *J. Vis. Exp.* **39**, e1787 (2010).
30. Shirendeb, U.P. *et al.* Mutant huntingtin's interaction with mitochondrial protein Drp1 impairs mitochondrial biogenesis and causes defective axonal transport and synaptic degeneration in Huntington's disease. *Hum. Mol. Genet.* **21**, 406–420 (2012).
31. Song, W. *et al.* Mutant huntingtin binds the mitochondrial fission GTPase dynamin-related protein 1 and increases its enzymatic activity. *Nat. Med.* **17**, 377–382 (2011).
32. Dang, M.T. *et al.* Disrupted motor learning and long-term synaptic plasticity in mice lacking NMDAR1 in the striatum. *Proc. Natl. Acad. Sci. USA* **103**, 15254–15259 (2006).
33. Ferrante, R.J., Beal, M.F., Kowall, N.W., Richardson, E.P. Jr. & Martin, J.B. Sparing of acetylcholinesterase-containing striatal neurons in Huntington's disease. *Brain Res.* **411**, 162–166 (1987).
34. Reiner, A. *et al.* Striatal parvalbuminergic neurons are lost in Huntington's disease: implications for dystonia. *Mov. Disord.* **28**, 1691–1699 (2013).
35. Hodges, A. *et al.* Regional and cellular gene expression changes in human Huntington's disease brain. *Hum. Mol. Genet.* **15**, 965–977 (2006).
36. Willson, T.M., Brown, P.J., Sternbach, D.D. & Henke, B.R. The PPARs: from orphan receptors to drug discovery. *J. Med. Chem.* **43**, 527–550 (2000).
37. Iwaisako, K. *et al.* Protection from liver fibrosis by a peroxisome proliferator-activated receptor–δ agonist. *Proc. Natl. Acad. Sci. USA* **109**, E1369–E1376 (2012).
38. Schilling, G. *et al.* Intranuclear inclusions and neuritic aggregates in transgenic mice expressing a mutant N-terminal fragment of huntingtin. *Hum. Mol. Genet.* **8**, 397–407 (1999).
39. Landis, S.C. *et al.* A call for transparent reporting to optimize the predictive value of preclinical research. *Nature* **490**, 187–191 (2012).
40. Perrin, S. Preclinical research: make mouse studies work. *Nature* **507**, 423–425 (2014).
41. Lu, M. *et al.* Brain PPAR-γ promotes obesity and is required for the insulin-sensitizing effect of thiazolidinediones. *Nat. Med.* **17**, 618–622 (2011).
42. Chiang, M.C., Chern, Y. & Huang, R.N. PPAR-γ rescue of the mitochondrial dysfunction in Huntington's disease. *Neurobiol. Dis.* **45**, 322–328 (2012).
43. Jin, J. *et al.* Neuroprotective effects of PPAR-γ agonist rosiglitazone in N171-82Q mouse model of Huntington's disease. *J. Neurochem.* **125**, 410–419 (2013).
44. Zheng, B. *et al.* PGC-1α, a potential therapeutic target for early intervention in Parkinson's disease. *Sci. Transl. Med.* **2**, 52ra73 (2010).
45. Shin, J.H. *et al.* PARIS (ZNF746) repression of PGC-1α contributes to neurodegeneration in Parkinson's disease. *Cell* **144**, 689–702 (2011).
46. Evans, R.M. & Mangelsdorf, D.J. Nuclear receptors, RXR, and the big bang. *Cell* **157**, 255–266 (2014).
47. Cramer, P.E. *et al.* ApoE-directed therapeutics rapidly clear β-amyloid and reverse deficits in AD mouse models. *Science* **335**, 1503–1506 (2012).
48. Fitz, N.F., Cronican, A.A., Lefterov, I. & Koldamova, R. Comment on "ApoE-directed therapeutics rapidly clear β-amyloid and reverse deficits in AD mouse models.". *Science* **340**, 924 (2013).
49. Gines, S. *et al.* Specific progressive cAMP reduction implicates energy deficit in presymptomatic Huntington's disease knock-in mice. *Hum. Mol. Genet.* **12**, 497–508 (2003).

ONLINE METHODS

Real-time (RT)-PCR analysis. RNA samples were isolated using Trizol (Life Technologies). Genomic DNA was removed using RNAse-free DNAse (Ambion). mRNA quantification was performed using the 7500 Real-Time PCR System (ABI) with ABI Assays-on-Demand primers and TaqMan-based probes. ABI TaqMan primer and probe set designations are available upon request. 18S RNA was used as an internal control. Relative expression levels were calculated via the $\Delta\Delta C_t$ method.

Cell culture and primary neuron studies. ST-*Hdh* cells were cultured as previously described[20]. Primary cortical neurons were prepared as previously described[50]. HEK293T cells were cultured as previously described[19,20]. HEK293T cells tested negative for mycoplasma contamination and were used for the purposes of preliminary testing, owing to their robust protein expression levels of transfected proteins, before confirmation of results in multiple physiologically relevant model systems. Cotransfection with the indicated constructs (previously described[19]) was done with Lipofectamine 2000, as per the manufacturer's protocol (Invitrogen). Addgene provided constructs for PPAR-α (plasmid no. 22751) and PPAR-γ (plasmid no. 8895). PPAR-δ–FLAG (Origene, MR207001) truncation constructs (encoding the following PPAR-δ variants: ΔA–C (deletion of residues 1–141), ΔA–D (deletion of residues 1–214), ΔD–F (deletion of residues 143–440) and ΔE–F (deletion of residues 215–440)) were made by standard techniques and verified by sequencing. Lentiviral transduction was used to induce gene expression or knockdown in primary neurons, with infection achieved by adding 1×10^7 titer units of lentivirus to the culture medium. For cotransfection assays, cells were drug-treated at 24 h after reporter transfection, harvested 24 h later and subjected to analysis using the Dual-Luciferase Reporter Assay system (Promega). Mitochondrial membrane potential in primary cortical neurons was measured via live-cell loading with a potential-sensitive dye, JC-1, using the Tecan M200Pro Reader. Analysis of cell death with immunofluorescence to activated caspase-3 and evaluation of MAP2 immunoreactivity to gauge neuron health were performed as described[51]. In all experiments, the investigator was blinded to culture conditions and cell treatments. Concentrations of compounds used: fenofibrate (Sigma, 100 nM), GW501516 (Santa Cruz, 100 nM), pioglitazone (Sigma, 20 nM) and H_2O_2 (Sigma, 25 μM).

Chromatin immunoprecipitation (ChIP). ChIP assays were performed as previously described[20]. Briefly, St-*Hdh* cells were cross-linked with 1% formaldehyde. After sonication, lysates were incubated with an antibody to PPAR-δ (sc-7197, Santa Cruz Biotechnology, 1:100) or control rabbit IgG (Santa Cruz Biotechnology, 1:100). Quantitative PCR analysis was performed with the SYBR Green PCR master mix (ABI) on a 7500 Real-Time PCR System (ABI).

Mouse studies. All animal experimentation adhered to NIH guidelines and was approved by, and performed, in accordance with the University of Washington Institutional Animal Care and Use Committee and the University of California San Diego Institutional Animal Care and Use Committee. The pCAGGS-*loxP*-STOP-*loxP* mouse wild-type *Ppard* transgenic construct[4] was mutated to yield *Ppard*^{E411P} (ref. 25), and then it was prepared for pronuclear injection. The resulting transgenic mice were crossed with *Cre*-hemizygous mice to derive floxed-STOP-*Ppard*^{E411P};*Cre* driver double-transgenic mice. All HD-transgenic, PPAR-δ–transgenic and *Cre*-driver lines were backcrossed onto the C57BL/6J strain background for >9 generations before genetic crosses were performed for purposes of experimentation. Blinded observers visually inspected mice for obvious neurological signs and examined mice with a composite neurological evaluation tool (ledge test, clasping, kyphosis and gait were scored on a scale of 0 (normal) to 3 (severely impaired)), as described previously[29]. Blinded investigators examined motor phenotypes by performing rotarod tests, as well as grip-strength and stride-length analyses, as previously described[20]. Cohort sizes were designated based upon power analysis for threshold effects of at least 25% difference. Novel-object recognition and Y maze–spatial memory testing were performed by blinded investigators as previously described[52].

For neuropathology experiments, brains were harvested as described[20]. Histopathology, volume measurements and stereology analysis were performed, as previously described[20]. For PPAR expression analysis, brain sections were incubated with antibodies to: NeuN (MAB377, Millipore; 1:100) and PPAR-δ (PA1-823A, Pierce; 1:200), PPAR-α (PA1-822A, Pierce; 1:200) or PPAR-γ (PA3-821A, Pierce; 1:200), and imaged with a Zeiss LSM 780 inverted microscope. Validation of PPAR-γ immunostaining of brain sections was achieved by detection of immunoreactivity in neurons of the hypothalamus, in agreement with previous work[41]. For electron microscopy analysis, brains were fixed, embedded and sectioned, and were then imaged with a Zeiss OM 10 electron microscope. Images were analyzed with the ImageJ program (NIH). In all cases, the scorer was blinded to the genotype status of the mice.

KD3010 pharmacology. KD3010 was injected intraperitoneally (15 mg/kg) as a suspension in corn oil (3 mg/ml) to fasted male C57BL/6J mice. Three cohorts of three mice each were dosed, and plasma and brains were taken at 2, 8 and 24 h and analyzed by liquid chromatography coupled to tandem mass spectrometry (LC-MS/MS) (AB Sciex API4000). For plasma samples, 10 μl of sample was treated with 100 μl dexamethasone in acetonitrile, the internal standard (IS) to precipitate protein, and the mixture was vortexed for 1 min and centrifuged at 13,000 r.p.m. for 15 min at 20–25 °C. 80 μl of the supernatant was then mixed with 160 μl water: acetonitrile (ACN) (95:5 vol:vol) with 0.1% formic acid (FA), vortex-mixed for 10 min and centrifuged for 10 min at 4,000 r.p.m. at 4 °C. 10 μl of sample was injected for LC-MS/MS analysis. Brain homogenates were prepared by homogenizing brain tissue for 2 min with 4 volumes (w:v) of homogenizing solution (deionized water). 60 μl of the sample was treated with 600 μl IS to precipitate protein, and the mixture was vortex-mixed for 1 min and centrifuged at 13,000 r.p.m. for 15 min at 20–25 °C. 80 μl of the supernatant was then mixed with 160 μl water:ACN (95:5 vol:vol) with 0.1% FA, vortex-mixed for 10 min and centrifuged for 15 min at 4,000 r.p.m. at 4 °C. 10 μl of sample was injected for LC-MS/MS analysis. A standard curve of KD3010 was determined with a lower limit of quantitation of 1 ng/ml for plasma and 5 ng/g for brain homogenate.

Treatment of mice with KD3010. After genotyping mice, we performed motor baseline assessment before group assignments, and littermates were randomly assigned to experimental groups while balancing genders, in accordance with guidelines intended to avoid spurious results[39,40]. Exclusion criteria determined before the start of the trial were: an adverse response to the injections or death before the start of treatment. These conditions did not occur. After group assignment, 6-week-old mice were injected daily, five times a week (from Monday to Friday), intraperitoneally with 50mg/kg/d of KD3010 suspended in corn oil (3 mg/ml). Blinded observers visually inspected mice for obvious neurological signs and examined mice with a composite neurological evaluation tool, as described previously[29]. Blinded investigators examined motor phenotypes by performing rotarod testing as previously described[20], as well as performing grip-strength and stride-length analysis[53]. Cohort sizes were designated based upon power analysis for threshold effects of at least 25% difference. For neuropathology experiments, brains were harvested as previously described[54,55]. Histopathology, volume measurements and stereology analysis were performed, as described previously[20]. In all cases, the scorer was blinded to the genotype status of the mice.

Bioenergetics assays. Mitochondrial complex activity assays were performed as described previously and adapted to a 96-well format[56]. For quantification of ATP, high-performance liquid chromatography (HPLC) of adenine nucleotides isolated from regions of the brain was performed, as done previously[20]. In all cases, the investigator was blinded to the genotype status of the mice.

Transcriptome analysis. RNA-sequencing (RNA-seq) analysis was performed by isolating RNA from the striatum of individual mice. The Illumina TruSeq RNA Sample Preparation Kit was used to prepare libraries for sequencing on the Illumina HiSeq 2000 system. RNA-seq data was mapped with the alignment software GSNAP to the mouse reference genome, which was obtained from NCBI (mm9, Build 37 assembly). The expression of genes was quantified by assigning reads to gene locations, as determined by the Ensembl gene annotations for mouse, and was subsequently normalized to the annotated gene length (exons only) and the depth of sequencing. Differentially expressed genes were called using the local *z*-score method on pair-wise sample comparisons, and they were

doi:10.1038/nm.4003

ranked by consistency of differential expression between similar comparisons of conditions. Order of magnitude threshold of 20%, a *P* value cut-off of 0.01 and a false-discovery rate of 0.005 were used to identify significantly altered genes by comparison of data from transgenic samples to those from nontransgenic controls. A representative subset of identified gene expression alterations was validated by qRT-PCR, as above. For gene ontology (GO) classification, differentially expressed genes in *Ppard*^{E411P} mice and in samples from humans with HD[35] were associated with the GO categories of cellular component and biological process. The GO-enriched biofunctional categories were compared using Ingenuity Pathway Analysis, and only GO categories with at least ten altered genes were reported and then ranked based upon the percentage of altered genes in a particular GO category.

Protein biochemistry analysis. The unbiased screen for HTT protein interactors was performed using a Panomics transcription factor (TF) immunoprecipitation array, according to the manufacturer's instructions (http://www.veritastk.co.jp/attached/2209/TFInteractionArrayKitcombined.pdf). HTT IP for the Panomics TF IP array used anti-HTT antibody EM48. Protein lysates were prepared as previously described[55]. For coimmunoprecipitations, homogenized protein was incubated with indicated coimmunoprecipitation antibody (GFP: 3E6 A11120, Life Technologies (1:100); HTT: MCA2050, Abcam (1:100); PPAR-δ: SC-7197, Santa Cruz; (1:100)). Proteins were run on 10% Bis-Tris gels (Invitrogen) and transferred to PVDF membranes (Millipore) before blocking in Odyssey Blocking Buffer (LI-COR Biosciences). Membranes were incubated with antibodies as indicated: anti-FLAG (F7425, Sigma; 1:1,000), anti-HTT (MAB2166, Millipore; 1:1,000), anti-GFP (A11121, Life Technologies, 1:1,000), anti–PPAR-δ (PA1-823A, Pierce; 1:1,000), anti–PPAR-α (PA1-822A, Pierce; 1:1,000), anti–PPAR-γ (PA3-821A, Pierce; 1:1,000) or anti–β-actin (ab8226, Abcam; 1:10,000), and imaged on the Odyssey instrument (LI-COR Biosciences). To obtain proteins *in vitro* for the measurement of direct interaction by coimmunoprecipitation, the Promega TnT T7 Quick Coupled Transcription/Translation System (Promega, #L1170) was used before coimmunoprecipitation.

Stem cell modeling. 60i4 HD induced pluripotent stem cells (iPSCs) were differentiated into medium spiny neurons for 56 d using a modified protocol[57], as described previously[58]. On day 42 of differentiation, cell aggregates were plated into 24-well plates coated with Matrigel (BD). Two weeks later, the cells were transferred to Neural Induction Medium (NIM). KD3010 or its enantiomer was added at the time of the medium change to NIM. After 48 h, cells were fixed with 4% paraformaldehyde in PBS for 30 min. After three washes with PBS, cells were stained with 0.8 μg/ml of Hoechst 33342 (Sigma) to visualize cell nuclei. A nuclear condensation assay to measure the extent of cell death was performed on three different clonal lines, as previously described[58].

Statistical analysis. Statistical analysis was done using Microsoft Excel, Prism 4.0 (GraphPad) or the VassarStats website (http://faculty.vassar.edu/lowry/VassarStats.html). For one-way analysis of variance (ANOVA), if statistical significance ($P < 0.05$) was achieved, we then performed post hoc analysis corresponding to the experiment, as specified in the figure legend, to account for multiple comparisons. Hypergeometric distribution analysis was performed using the Stat Trek calculator (http://stattrek.com/online-calculator/hypergeometric.aspx). All *t*-tests were two-tailed Student's *t*-tests unless otherwise indicated, and the level of significance (alpha) was always set at 0.05.

50. Young, J.E., Martinez, R.A. & La Spada, A.R. Nutrient deprivation induces neuronal autophagy and implicates reduced insulin signaling in neuroprotective autophagy activation. *J. Biol. Chem.* **284**, 2363–2373 (2009).
51. Young, J.E. *et al.* Polyglutamine-expanded androgen receptor truncation fragments activate a Bax-dependent apoptotic cascade mediated by DP5 (Hrk). *J. Neurosci.* **29**, 1987–1997 (2009).
52. Nithianantharajah, J., Barkus, C., Murphy, M. & Hannan, A.J. Gene-environment interactions modulating cognitive function and molecular correlates of synaptic plasticity in Huntington's disease transgenic mice. *Neurobiol. Dis.* **29**, 490–504 (2008).
53. Sopher, B.L. *et al.* Androgen receptor YAC–transgenic mice recapitulate SBMA motor neuronopathy and implicate VEGF164 in the motor neuron degeneration. *Neuron* **41**, 687–699 (2004).
54. Garden, G.A. *et al.* Polyglutamine-expanded ataxin-7 promotes non–cell-autonomous Purkinje cell degeneration and displays proteolytic cleavage in ataxic transgenic mice. *J. Neurosci.* **22**, 4897–4905 (2002).
55. La Spada, A.R. *et al.* Polyglutamine-expanded ataxin-7 antagonizes CRX function and induces cone-rod dystrophy in a mouse model of SCA7. *Neuron* **31**, 913–927 (2001).
56. Janssen, A.J. *et al.* Spectrophotometric assay for complex I of the respiratory chain in tissue samples and cultured fibroblasts. *Clin. Chem.* **53**, 729–734 (2007).
57. Aubry, L. *et al.* Striatal progenitors derived from human ES cells mature into DARPP32 neurons *in vitro* and in quinolinic acid–lesioned rats. *Proc. Natl. Acad. Sci. USA* **105**, 16707–16712 (2008).
58. HD iPSC Consortium. Induced pluripotent stem cells from patients with Huntington's disease show CAG-repeat expansion–associated phenotypes. *Cell Stem Cell* **11**, 264–278 (2012).